Carrier injection by static induction mechanism in MLE-grown planar-doped barrier n+-i-p+-i-n+ structures

著者	小山　裕
journal or publication title	IEEE Transactions on Electron Devices
volume	44
number	1
page range	195-197
year	1997
URL	http://hdl.handle.net/10097/46406

doi: 10.1109/16.554811

Briefs

Carrier Injection by Static Induction Mechanism in MLE-Grown Planar-Doped Barrier n^+-i-p^+-i-n^+ Structures

Y. X. Liu, P. Plotka, K. Suto, Y. Oyama, and J. Nishizawa

***Abstract*—The I–V characteristics of GaAs n^+-i-p^+-i-n^+ diode structures grown by MLE with source-drain distances from 500 Å to 950 Å have been measured at temperatures ranging from 77 K to 423 K. The analysis of experimental results indicates that the current flows over the static-induction-controlled potential barrier. On this basis, quantitative comparison with thermionic emission theory which assumes injection of ballistic electrons are made.**

I. Introduction

A purely semiconductor device with the ballistic transport was proposed by Nishizawa [1], [2] following the proposal of Static Induction Transistor (SIT). In order to realize ideal SIT with the ballistic transport, Nishizawa and coworkers developed molecular layer epitaxy (MLE) of gallium arsenide [3]. The planar-doped barriers (PDB) in GaAs grown by MBE have been reported [4]–[6]. However, the analysis of I–V characteristics was confined at room temperature, and the samples with thicknesses larger than 1000 Å were used. In this paper, we report the comparison of experimental and theoretical I–V characteristics of PDB diode structures grown by MLE [7], [8] with electrically measured source-drain distances from 500 Å to 950 Å at temperatures ranging from 77 K to 423 K. We confirm the basic relation of static induction mechanism that the sum of inverse of intrinsic voltage amplification factors nearly equals unity (larger than 0.9) for every sample type above room temperature region. On this basis, the experimental forward currents are described by thermionic emission theory with $\gamma_F A^*$ instead of the effective Richardson constant A^*, where γ_F is the ballistic injection factor. The estimation and evaluation of the values γ_F for various diodes are made.

II. Current Flow Mechanism

The schematic diagram of the PDB diode structure and a one dimensional (1-D) diagram of the potential distribution at forward condition are illustrated in Fig. 1(a) and (b). The potential barrier height in the device is approximately determined by the area density of ionized acceptors in the p^+ layer with only a few monolayer thicknesses and geometrical structures [4]. If external voltage is applied to the drain, the height of potential barrier and in turn the drain current can be changed by the drain voltage $(V_{\rm DS})$ through static induction [1].

First, it should be noted that the effective Richardson constant A^* is applicable when the electron energy is low enough, that the effective mass m^* can be assumed to have a constant value. However, there is finite potential barrier in the channel region.

Manuscript received December 28, 1995; revised July 20, 1996. The review of this brief was arranged by Editor P. M. Solomon.

Y. X. Liu, K. Suto, and Y. Oyama are with the Department of Materials Science and Engineering, Faculty of Engineering, Tohoku University, Sendai 980, Japan.

P. Plotka is with the Semiconductor Research Institute, Sendai 980, Japan.

J. Nishizawa is with Tohoku University, Sendai 980, Japan.

Publisher Item Identifier S 0018-9383(97)00324-9.

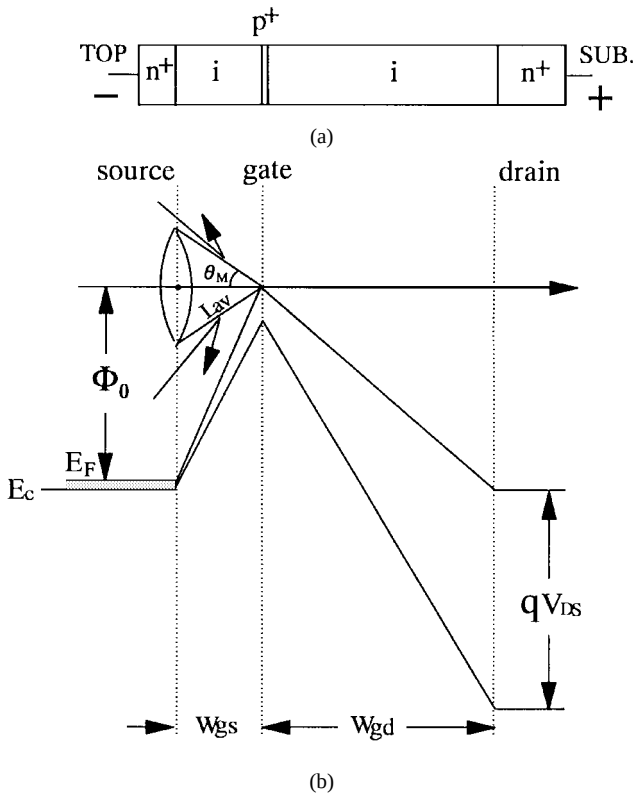

Fig. 1 (a) Schematic illustration of planar-doped barrier diode structure. (b) Schematic diagram of potential distribution and the maximum ballistic solid angle.

Second, the directions of the electrons, which are injected from source to channel are distributed in three-dimensional (3-D) space as schematically illustrated in Fig. 1(b). So that only the electrons in a narrow directional cone can reach the intrinsic gate without collision, otherwise experience scattering. Considering above facts, the experimental forward current can be described as

$$I_F \simeq \gamma_F S A^* T^2 \exp\left(-\frac{q\phi_0}{k_B T}\right) \exp\left(\frac{qV_{\rm DS}}{\mu_F^* k_B T}\right) \qquad (1)$$

where γ_F is the ballistic injection factor, S is device area, A^* is the effective Richardson constant for GaAs (8.16 A/cm^{2}K^2), Φ_0 is barrier height at zero bias, $\mu_F^*(\approx 1 + W_{\rm gd}/W_{\rm gs})$ is intrinsic voltage amplification factor [1], $W_{\rm gs}$ and $W_{\rm gd}$ are the distances for source-gate and gate-drain, and k_B is the Boltzmann constant. The values of γ_F and Φ_0 for each diode can be obtained by measuring the temperature dependence of saturation current. The experimental reverse current can be similarly expressed with $\mu_R^*(\approx 1 + W_{\rm gs}/W_{\rm gd})$ instead of μ_F^*.

III. Experimental Result and Discussion

The GaAs planar-doped barrier n^+-i-p^+-i-n^+ diode structures were grown by MLE, using selenium and zinc as n^+ and p^+ dopants, respectively, and about forty testing diodes with an area of $120\ \mu$m $\times 120\ \mu$m were formed on each sample wafer. Among them, the designed parameters for three typical groups of samples are tabulated

TABLE I
DESIGNED AND EXPERIMENTAL PARAMETERS IN MLE

parameters	type A sample	type B sample	type C sample
N_S [cm^{-3}]	5×10^{18}	5×10^{18}	2×10^{19}
W_{gs0} [Å]	200	200	60
N_p [cm^{-2}]	2.3×10^{12}	3.0×10^{12}	8.1×10^{12}
W_{gd0} [Å]	800	800	400
N_D [cm^{-3}]	5×10^{18}	5×10^{18}	5×10^{18}
Φ_{00} [mV]	497	662	583
Φ_0 [mV]	502	618	648

in Table I, where N_p is the area density of Zn doping, $W_{\rm gs0}$ and $W_{\rm gd0}$ are designed geometrical distances for source-gate and gate-drain, Φ_{00} is the calculated barrier height from $N_p, W_{\rm gs0}$ and $W_{\rm gd0}$ [4], Φ_0 is measured barrier height, and N_S and N_D are the doping concentrations of source and drain region. By C–V measurement, we confirmed that the total depletion layers were about 950 Å for both of type A and B samples, and about 500 Å for type C samples, as well as the value of N_D was confirmed to be 5.2×10^{18} $\rm cm^{-3}$, which nearly equals to designed values as shown in Table I. On the other hand, by the dynamic SIMS measurement, the broaden width of the planar-like Zn doping layer was confirmed to be smaller than $\sim$30 Å, which value corresponds to the depth resolution of the dynamic SIMS.

The I–V characteristics for samples with type A, B, and C were measured and analyzed. Above room temperature region, there is a good agreement between experimental and calculated I–V characteristics by using (1) for all samples at both forward and reverse conditions. The values for $\Phi_0, \gamma_F, 1/\mu_F^*, 1/\mu_R^*$ determined by experiment were used above calculation. Below room temperature, the experimental values of current gradually deviated from the calculated ones with lowering temperature.

The experimental determinations of the parameters for $1/\mu_F^*, 1/\mu_R^*, \Phi_0$, and γ_F were made as follows. From the slopes of the experimental I–V characteristics for both forward and reverse bias voltages in semi-log plots at nearly linear regions, the inverse of intrinsic amplification factors $1/\mu_F^*$ and $1/\mu_R^*$ for all samples were obtained at given temperatures and plotted as a function of temperature as shown in Fig. 2. It is clear that experimental values of $1/\mu_F^*$ and $1/\mu_R^*$ are close to designed ones as dash dot lines shown in Fig. 2. The sum of $1/\mu_F^* + 1/\mu_R^*$ are found to be close to unity, i.e., larger than 0.9 for all samples above room temperature region. These results ascertain that the carriers are injected over the static-induction-controlled potential barrier above room temperature region.

The parameters Φ_0 and γ_F were measured from the dependence of $\ln(I_s/T^2) - 1/T$ plot, here I_s is the current extrapolated the experimental $\ln(I_F) - V_{\rm DS}$ plots to zero bias voltage. Actually the experimental data for all samples exhibited nearly linear behavior above room temperature region as the solid lines shown in Fig. 3. So that the values Φ_0 and γ_F are obtained as $\Phi_0 = 502$ mV, 618 mV, 648 mV, and $\gamma_F = 7.4\%, 0.3\%, 0.8\%$ for type A, B, and C samples, respectively. Below room temperature, the experimental data points deviated from the linear dependence, and the deviation is more pronounced for samples with type C which has the smallest structure among these three samples. Such behavior probably due to the electron tunneling through the potential barrier.

As a result, the experimentally determined values γ_F for every sample are less than what are predicted by a simple thermionic emission theory. Relatively better agreement is obtained for type A sample ($\gamma_F = 7.4\%$). This is reasonable because its potential barrier is the lowest among those of the three samples. Considering that μ_F^* is around 4, the potential barrier for type A sample becomes less than 0.31 eV when the applied voltage $V_{\rm DS}$ exceeds about 0.8 V. Even in this case the average value of the effective mass m^* will

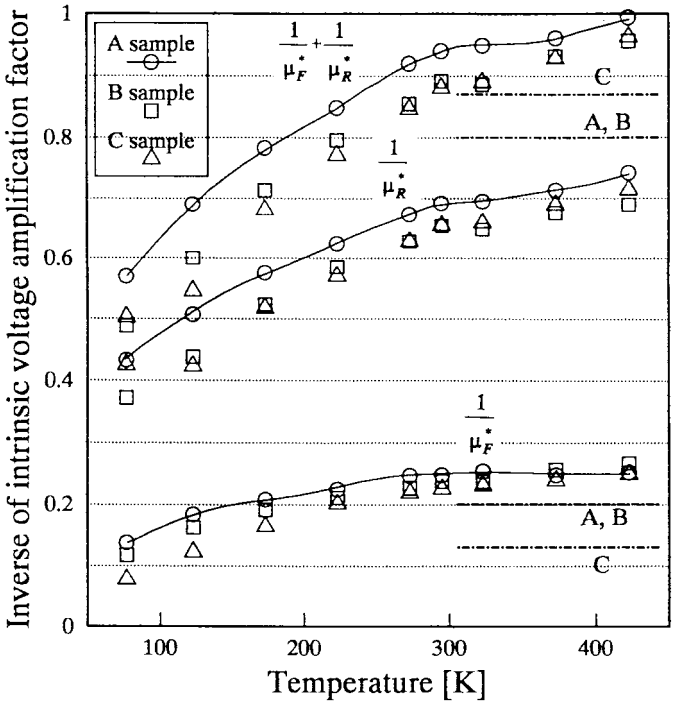

Fig. 2. Temperature dependence of the inverse of intrinsic voltage amplification factors and their sum.

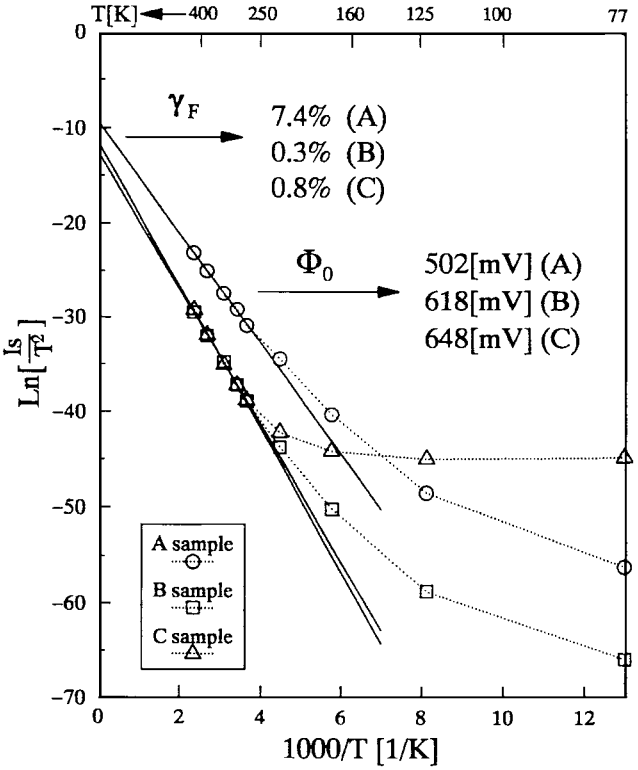

Fig. 3. Activation energy plots for determination of barrier height Φ_0 and ballistic injection factor γ_F.

be smaller than those at the bottom of conduction band. For type B and C samples, nonparabolicity of the conduction band will be more severe, because of the higher value of Φ_0.

Another factor which should have caused a discrepancy from the simple thermionic emission equation is the effect of scattering. Although the scattering mechanisms are complex, as a crude approximation, we assume that only a portion of electrons within a narrow directional cone as shown in Fig. 1(b) can reach the intrinsic gate without collision, otherwise they will experience scattering and will not contribute to the thermionic emission current. Then the maximum ballistic solid angle can be expressed by $2\pi\theta_M = 2\pi\cos^{-1}(W_{\rm gs}/L_{\rm av})$, where $L_{\rm av}$ is the mean free path of electrons. Because the mean free path will be much smaller with increasing electron energy due to excitation of optical phonons, the above equation can not be applicable in real situations. However, at least it can be said that the effect of the scattering will be severe when $W_{\rm gs}$ becomes close to some critical value corresponding to the mean free path. In our PDB diode structure, $W_{\rm gs}$ for type A and B samples is the same and is almost three times larger than that for type C sample, and the potential barrier height Φ_0 for type A sample is the lowest among these three samples. So that the differences in the experimentally determined values γ_F for three type samples, 7.4% (A), 0.3% (B), 0.8% (C), can be explained qualitatively. For more quantitative discussion of the ballistic transport factor, diode structures with further lower potential barriers will be necessary to eliminate the complexity of the GaAs band structure.

IV. Conclusion

The I–V characteristics of GaAs PDB diode structures grown by MLE with electrically measured source-drain distances from 500 Å to 950 Å have been measured at temperatures ranging from 77 K to 423 K. The carrier injection by static induction mechanism was confirmed experimentally. The small values of γ_F were explained qualitatively by the nonparabolicity of the band structure and scattering which confines the ballistic electrons within the maximum ballistic solid angle. It means that to get larger γ_F, the barrier height Φ_0 should be designed lower. At low temperature, the current probably due to tunneling requires further study.

Acknowledgment

The authors would like to thank Dr. Kurabayashi, and Mr. Kikuchi and Mr. Henmi for the fabrication of MLE sample wafers.

References

[1] J. Nishizawa, T. Terasaki, and J. Shibata, "Field-effect transistor versus analog transistor (static induction transistor)," *IEEE Trans. Electron Devices*, vol. ED-22, pp. 185–197, 1975.
[2] J. Nishizawa and K. Motoya, "SIT as ballistic device," *Topics in Millimeter Wave Technology*, K. J. Button, Ed. New York: Academic, 1988, vol. 2, pp. 213–247.
[3] J. Nishizawa, H. Abe, and T. Kurabayashi, "Molecular layer epitaxy," *J. Electrochem. Soc.*, vol. 132, pp. 1197–1200, 1985.
[4] R. J. Malik, T. R. Aucoin, R. T. Ross, K. Board, C. E. C. Wood, and L. F. Eastman, "Planar-doped barriers in GaAs by molecular beam epitaxy," *Electron. Lett.*, vol. 16, pp. 836–837, 1980.
[5] R. F. Kazarinov and S. Luryi, "Charge injection over triangular barriers in unipolar semiconductor structures," *Appl. Phys. Lett.*, vol. 38, no. 10, pp. 810–812, 1981.
[6] A. C. Gossard, R. F. Kazarinov, S. Luryi, and W. Wiegmann, "Electric properties of unipolar GaAs structures with ultrathin triangular barriers," *Appl. Phys. Lett.*, vol. 40, no. 9, pp. 832–833, 1982.
[7] P. Plotka, T. Kurabayashi, Y. Oyama, and J. Nishizawa, "Ideal static induction transistor implemented with molecular layer epitaxy," *Appl. Surf. Sci.*, vol. 82/83, pp. 91–96, 1994.
[8] Y. Oyama, P. Plotka, and J. Nishizawa, "Selective MLE growth of GaAs and surface treatment for ideal static induction transistor (ISIT) application," *Appl. Surf. Sci.*, vol. 82/83, pp. 41–45, 1994.

Dependence of the Injection Current at Lasing Threshold on Structure and Losses in AlGaN/GaN Lasers

Pankaj Shah and Vladimir Mitin

***Abstract*— We present calculations of the threshold current densities, $J_{\rm th}$, in AlGaN/GaN double heterostructure lasers for different active region thickness, losses, and cavity lengths. Two-dimensional (2-D) numerical simulations indicate that for a 100-μm long cavity, a 0.1-μm thick active region gives the lowest $J_{\rm th}$ when only mirror losses are present. As losses increase, the minimum moves to thicker active regions. $J_{\rm th}$ versus optical loss plots demonstrate that with the high optical losses in the materials grown, it will be easier to induce lasing in thick active region structures. Results for AlGaAs/GaAs lasers presented for comparison, demonstrate that AlGaN/GaN lasers have higher $J_{\rm th}$ unless the active region is very thin.**

I. Introduction

There is great interest in creating current injection pumped semiconductor lasers from the wide bandgap AlInGaN material system to obtain short wavelength light [1], [2]. Due to difficulties in growing high quality materials, this goal has only recently been achieved [3], [4]. Other devices based on the wide bandgap materials, such as light emitting diodes [5]–[7], transistors [8], and detectors [9], have been demonstrated. Numerical simulations of nitride based lasers are needed to give experimentalists some indication of the threshold currents expected with the materials available. There have been several theoretical predictions of gain and threshold currents in nitride based wide bandgap lasers [10]–[13]. However, these theoretical works have not taken into account the complete structure of the laser, and important factors such as charge carrier emission at heterojunctions, current spreading and carrier leakage out of the active region.

We have previously simulated InGaN/AlGaN light emitting diodes [14] and obtained results which agreed well with experiments, demonstrating that numerical simulations of wide bandgap nitride based semiconductor devices can aid in their development. We have now performed 2-D numerical simulations of semiconductor lasers using a version of the MINILASE [15] program which we have modified for wide bandgap laser simulations.

II. Simulation Procedure and Device Structure

The simulation program solves, over a 2-D cross section of the device, Poisson's equation, the electron and hole continuity equations, and the wave equation. Thermionic emission is included for electrons

Manuscript received February 23, 1996; revised August 8, 1996. The review of this brief was arranged by Editor P. K. Bhattacharya. This work was supported by the Army Research Office.

The authors are with the Department of Electrical and Computer Engineering, Wayne State University, Detroit, MI 48202 USA.

Publisher Item Identifier S 0018-9383(97)00325-0.